THE JOURNAL OF PHYSICAL CHEMISTRY B
A JOURNAL OF THE AMERICAN CHEMICAL SOCIETY

pubs.acs.org/JPCB

Article

Quantitative Multistate Binding Model of Silica Nanoparticle−Protein Interactions Obtained from Multinuclear Spin Relaxation

Gregory Jameson, Xinyao Xiang, and Rafael Brüschweiler*

Cite This: *J. Phys. Chem. B* 2022, 126, 9089−9094

Read Online

ACCESS | Metrics & More | Article Recommendations

ABSTRACT: Nanoparticle-assisted NMR spin relaxation (NASR), which makes internal protein dynamics in solution directly observable on nanosecond to microsecond time scales, has been applied to different nuclei and relaxation processes of the same protein system. A model is presented describing the transient interaction between ubiquitin and anionic silica nanoparticles for the unified interpretation of a wealth of experimental data including ^{2}H, ^{13}C, and ^{15}N relaxation of methyl side chain and backbone moieties. The best model, implemented using a stochastic Liouville equation, describes the exchange process via an intermediary encounter state between free and fully nanoparticle-bound protein. The implication of the three-state binding model on the interpretation of NASR data is discussed.

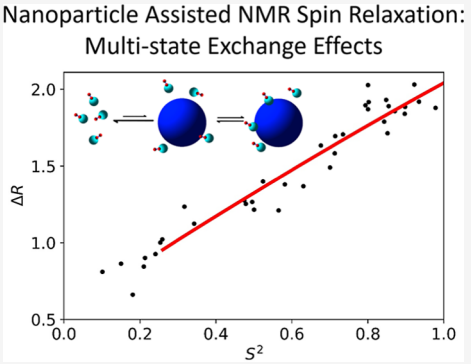

INTRODUCTION

The emergence of nanoscience applications in biology, especially in biomedicine, including drugs, drug carriers, or imaging agents,[1,2] demands a detailed understanding of the interactions between synthetic nanoparticles and biological molecules.[3−5] In biological applications, nanoparticles are inevitably exposed to in vivo environments where a vast array of diverse native biomolecules exist, encompassing proteins, nucleic acids, membranes, and metabolites. The complex nature of such nanoparticle−biomolecule interactions is well recognized.[6,7] Nuclear magnetic resonance (NMR) spectroscopy in solution is uniquely suited to report on nanoparticle−protein interactions.[8−19] Such interactions can range from essentially permanent to highly transient with rapid exchange between free and nanoparticle-bound states. However, the experimental characterization of such transient interactions between proteins and nanoparticles remains challenging due to the elusive nature of the bound state(s).

From a solution NMR perspective, a molecule with long-lived interactions with large particles or nanostructures will have a very large linewidth accompanied by low sensitivity impeding the direct observation of such complexes. This is a consequence of the rate of rotational Brownian diffusion that slows down with increasing particle size. However, in case that these interactions are transient, experiencing sufficiently rapid exchange, and have bound populations on the order of a few percent or even smaller, the resulting protein NMR spectra will still have a solution-NMR-like appearance with high spectral resolution and good sensitivity. At the same time, these spectra encode unique information about properties of the nanostructure, the exchange process, and the protein molecule itself. Multiple NMR methods exist that are able to characterize the interaction between the free state and a large, much more slowly tumbling bound state. These techniques include the transferred nuclear Overhauser effect,[20−22] enhanced water relaxation through exchange,[23,24] saturation transfer difference NMR,[25,26] paramagnetic relaxation enhancement,[27,28] and dark-state exchange saturation transfer (DEST).[29,30] We recently introduced nanoparticle-assisted spin relaxation (NASR), which exploits the difference in relaxation between free protein and the protein in the presence of nanoparticles to report about internal dynamics on time scales exceeding the tumbling correlation time τ_p of the free protein by several orders of magnitude in a structure-independent manner.[9,10] NASR covers the well-known "blind spot" of traditional solution NMR spin relaxation on time scales from nanosecond to microsecond. Additionally, this difference in relaxation also depends on the kinetics of binding when more sophisticated motional models are used for spin relaxation data interpretation.[31]

Received: August 19, 2022
Revised: October 2, 2022
Published: October 31, 2022

https://doi.org/10.1021/acs.jpcb.2c05967
J. Phys. Chem. B 2022, 126, 9089−9094

In our recent work, we presented a set of NASR experiments utilizing methyl $^{13}C-^{1}H$ dipole−dipole cross-correlation rates Γ and methyl ^{2}H transverse relaxation rates $R(D_+)$ (abbreviated as R_+ below) for ubiquitin, henceforth referred to as generic relaxation rates R.[32] There we noted a systematic positive offset in the linear correlation of NASR rates versus Lipari−Szabo order parameter ${S_{axis}}^2$. A simple two-site exchange model predicts that NASR relaxation rates follow the relationship[9]

$$\Delta R \propto p_B \tau_{NP} S^2 \tag{1}$$

where p_B is the bound population, τ_{NP} is the global correlation time of the nanoparticle-bound state, and the proportionality constant is dependent on the nuclei involved as well as the underlying spin relaxation mechanism. As a result, the observed offset in the linear relationship between ΔR versus S^2 cannot be explained by the above relationship. Further analysis showed no dependence on the external magnetic B_0 field and several potential origins could be excluded as the source of this behavior, such as residue-specific interactions with nanoparticles, increased viscosity, or paramagnetic relaxation. Additionally, the ratio of NASR methyl-$\Delta R_+(^2H)$ versus backbone $\Delta R_2(^{15}N)$ is markedly different than that predicted by eq 1. This situation calls for a more detailed model to obtain a unified description of nanoparticle-assisted spin relaxation in ubiquitin for all three relaxation processes with the goal to obtain a more detailed understanding of the nature of protein−nanoparticle binding (Figure 1).

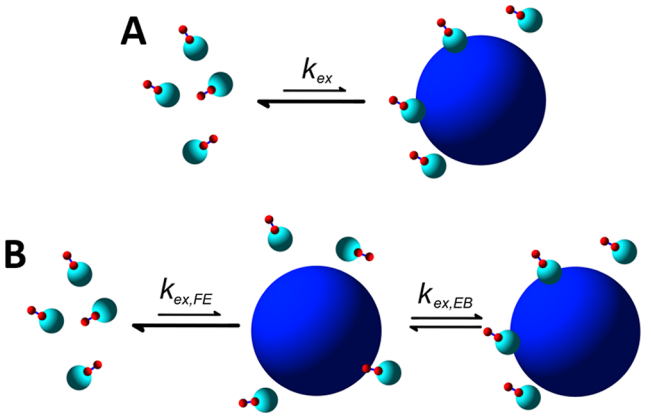

Figure 1. Depiction of the two-state (A) and three-state (B) exchange models for the interaction of proteins with nanoparticles used in this work. In the two-state model, the protein can adopt two states: a free state ("F") where it tumbles with a correlation time as in free solution and a nanoparticle-bound state ("B") where it tumbles with the much slower correlation time of the nanoparticle. In the three-state model, the protein can in addition be in an intermediate "encounter state" ("E") where the protein interacts with the nanoparticle more loosely, thus retaining some mobility with the rotational correlation time slowing down while being still faster than that of the nanoparticle itself.

We recently developed a stochastic Liouville equation (SLE) as a more advanced theoretical description of NASR data.[31] It combines spin evolution, Brownian rotational tumbling of the free and bound state, internal dynamics, and exchange kinetics of a system in a single differential equation. The SLE has two major advantages over classical relaxation theory: first, it is accurate for molecules of any size or rotational correlation times, including those outside the Redfield regime,[33] and second, it can be used to describe exchange kinetics on any time scale. In our previous work, this formalism was used to quantify the effects of binding kinetics and the size of interaction partners on the spin relaxation of different types of nuclear spins of proteins. In particular, it was found that a "sweet spot" of exchange rates k_{ex} between 10^3 and 10^6 s^{-1} was optimal for detecting substantial NASR effects.[31] However, that work did not attempt quantitative comparisons with experimental data. As classical relaxation theory fails to fully explain the NASR effects in the case of ubiquitin mentioned above, the more generalized SLE-based theory presents itself as a powerful numerical approach for the rigorous treatment of these relaxation effects in a unified manner.

MATERIALS AND METHODS

The ubiquitin NASR data, which were measured as described previously,[32] are depicted in Figure 2 as black dots. The linear trend between differential NASR relaxation rates and traditional S^2 model-free order parameters can be seen clearly in both the ^{13}C $\Delta\Gamma$ and ^{2}H ΔR_+ profiles with both exhibiting a positive non-zero offset. However, due to the limited range of S^2 for the majority of ^{15}N peaks, this trend is much less pronounced for ^{15}N ΔR_2.

As the SLE calculations are a rather time-intensive process (it takes approximately 1 cpu h per S^2 value for all three relaxation processes on a local computer cluster with 16 cores), and given the strong linear relationship between S^2 and ΔR in ^{13}C Γ and ^{2}H R_+, a limited set of S^2 was used for fitting. For $\Delta\Gamma(^{13}C)$ and $\Delta R_+(^2H)$, four S^2 values of S^2 = 0.25, 0.5, 0.75, and 1.0 were chosen for SLE calculations, along with a projected S^2 = 0.0 value determined from a linear fit of the other four points. For $\Delta R_2(^{15}N)$, only one S^2 value of 0.85 was chosen due to the limited experimental range of this parameter in ubiquitin, with a fivefold stronger weight than each S^2 value of the other nuclei to ensure its appropriate weighting in the final fitting result. Differences between calculated and experimental values were then normalized to the experimental magnitude of ΔR for that relaxation process at S^2 = 1.0. This results in the following scoring function

$$\chi^2 = \sum_{S^2=0,0.25,0.5,0.75,1} \left(\frac{\Delta\Gamma_{exp}(^{13}C, S^2) - \Delta\Gamma_{SLE}(^{13}C, S^2)}{\Delta\Gamma_{exp}(^{13}C, 1.0)} \right)^2 + \sum_{S^2=0,0.25,0.5,0.75,1} \left(\frac{\Delta R_{+,exp}(^{2}H, S^2) - \Delta R_{+,SLE}(^{2}H, S^2)}{\Delta R_{+,exp}(^{2}H, 1.0)} \right)^2 + 5 \left(\frac{\Delta R_{2,exp}(^{15}N, 0.85) - \Delta R_{2,SLE}(^{15}N, 0.85)}{\Delta R_{2,exp}(^{15}N, 1.0)} \right)^2 \tag{2}$$

and fitting was performed via the Nelder−Mead simplex algorithm.[34]

RESULTS AND DISCUSSION

Initially, we started with a two-state free/bound model (Figure 1A) for fitting of the data with the best fitting results shown in Figure 2. The free-state global protein tumbling correlation time τ_P was fixed using free-state data at τ_P = 4.094 ns. The optimal fit of the data with this model, plotted as blue lines in Figure 2, has a nanoparticle-bound rotational correlation time τ_{NP} = 932 ns, an exchange rate k_{ex} = 4850 s^{-1}, and a bound

https://doi.org/10.1021/acs.jpcb.2c05967
J. Phys. Chem. B 2022, 126, 9089−9094

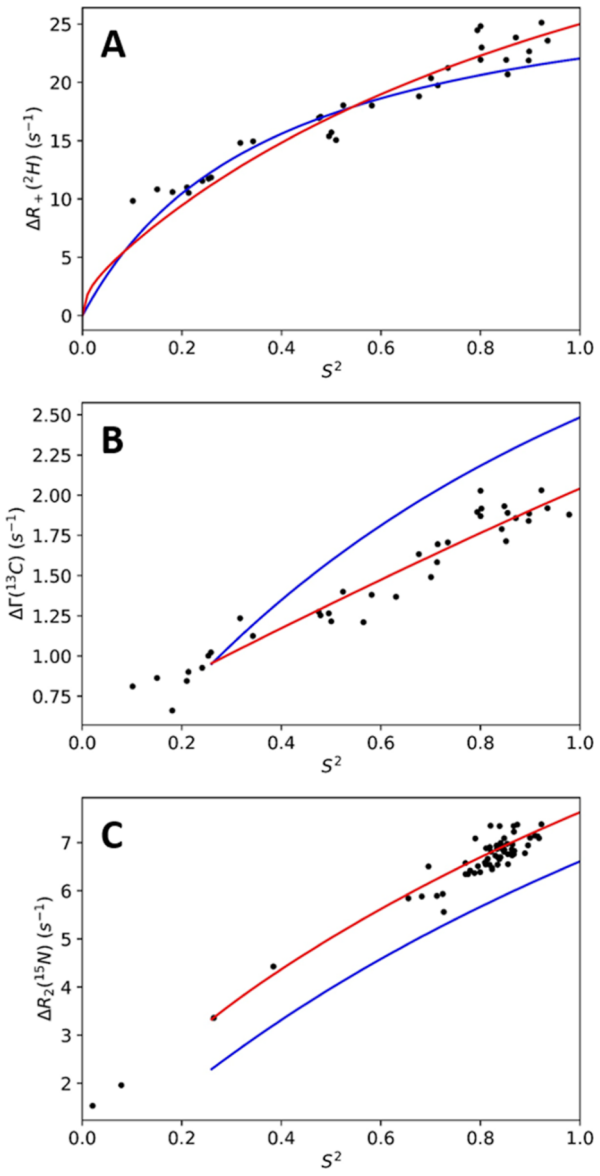

Figure 2. NASR ΔR values plotted against model-free order parameter S^2 for the following: (A) $\Delta R_+(^2H)$, (B) $\Delta\Gamma(^{13}C)$, and (C) $\Delta R_2(^{15}N)$. Experimental data are indicated by black circles. The lines indicate back-calculated relaxation values via SLE using the best fit parameters for the two-state (blue) and three-state (red) model. Note that for $S^2 = 0$, the predicted $\Delta R = 0$.

population $p_B = 0.627\%$. Several issues were identified when comparing the fit with the experimental data. First, a substantial curvature can be seen in the theoretical $\Delta R_+(^2H)$ values, including in the range where the experimental linear correlation is strongest. Second, the theoretical values for $\Delta\Gamma(^{13}C)$ at high S^2 are too large, while the values for $\Delta R_+(^2H)$ and $\Delta R_2(^{15}N)$ are too small. As a result, the quality of the fits is unsatisfactory, indicating that the simple two-state model needs improvement.

A more complex model is the three-state model of Figure 1B with an on-pathway intermediate state between the free and the fully nanoparticle-bound states. Such an interaction model has previously been discussed in the context of DEST experiments on other systems involving transient binding to a large state.[35,36] This intermediate state is labeled the "encounter complex state" (abbreviated E) and can have substantially slower tumbling for the protein than in its free form as it is transitioning from the free (F) state to the bound (B) state. Such a scenario has been described as a protein interacting with the hydration layer surrounding the nanoparticle.[36] Alternatively, the tumbling properties of this state may also be dominated by effects such as an increase in local viscosity[37] or weak interactions with the nanoparticle as the protein reorients itself into favorable binding orientations.

Fitting of the three-state model performs qualitatively and quantitatively much better than of the two-state model, with the best fitting results compiled in Table 1. The fitted

Table 1. Best Fit Model Parameters and Their Error Estimates

fitting parameter	best fit value	error
encounter state correlation time, τ_E (ns)	288	47
bound rotational correlation time, τ_B (ns)	1080	420
free-to-encounter exchange rate, $k_{ex,FE}$ (s^{-1})	4440	660
encounter-to-bound exchange rate, $k_{ex,EB}$ (s^{-1})	340	110
encounter population, p_E (%)	1.14	0.18
bound population, p_B (%)	2.04	0.35

relaxation curves with the best fit parameters are shown in Figure 2 as red curves. The $\Delta R_2(^{15}N)$ and $\Delta\Gamma(^{13}C)$ values are outstanding fits, and the $\Delta R_+(^2H)$ are well explained in the medium to high S^2 range where most experimental data points are found with the lowest few S^2 values exhibiting minor discrepancies.

The large set of experimental NASR data available for ubiquitin from different types of nuclei, namely, ^2H, ^{13}C, and ^{15}N, requires a self-consistent dynamic model for the description of the transient interactions of the protein with anionic silica nanoparticles. With NASR depending on the tumbling rates of the free and bound states, the internal dynamics of the protein, and the exchange parameters, implementation of a model requires a comprehensive framework provided by the SLE. It is found that the simple two-state binding model is only qualitatively useful as it fails to quantitatively explain the relaxation behavior measured for ubiquitin. The three-state model provides a substantially improved agreement with the experiment (Figure 2). Moreover, the numerical values of the best fit-model parameters are physically sensible. Notably, the bound rotational correlation time is very close to the theoretical correlation time of 910 ns predicted by the Stokes−Einstein−Debye equation for nanoparticles with a 20 nm diameter in H_2O used for the experiments. The small bound population (2.04%) is also reasonable as it is consistent with the previously observed invariance of longitudinal relaxation rates in the presence and absence of nanoparticles.[32] Finally, the free-to-encounter rate of approach, $k_{FE} = 51.7\ s^{-1}$, is well within the diffusion limit of $k_{FE,diff} = 1270\ s^{-1}$ determined according to Alberty and Hammes.[38]

In our previous work on the modeling of NASR data using SLE, it was noted that relaxation rates behave similarly for fast and slow exchange rates. The threshold between "slow" and "fast" is proportional to the strength of the anisotropic-relaxation-active interaction,[31] which places the exchange rates obtained here in the slow regime. The simultaneous use of relaxation data for multiple nuclei breaks the degeneracy between slow and fast rates as the anisotropic spin interaction strengths differ among these relaxation processes (i.e.,

https://doi.org/10.1021/acs.jpcb.2c05967
J. Phys. Chem. B 2022, 126, 9089−9094

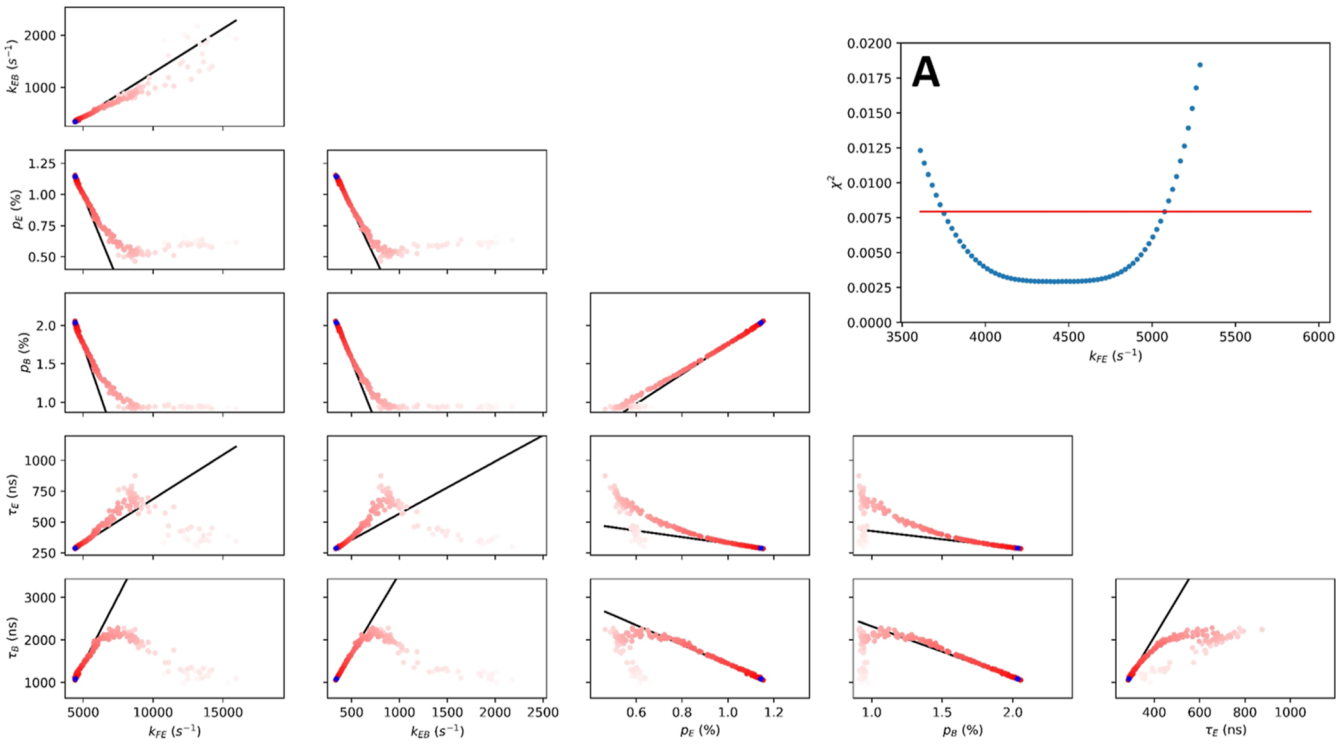

Figure 3. Fitting trajectories of the three-state model using the Nelder−Mead fitting algorithm. Red points indicate points visited in the simplex in the two-dimensional subspaces spanned by pairs of model parameters k_{FE}, k_{EB}, p_E, p_B, and τ_E. More faint points belong to earlier parts of the trajectory and blue points indicate the final simplex. The black lines indicate 1D "valleys" in the fitting space of degenerate parameter sets with minimal χ^2. Inset (A) plots parameter χ^2 of points within the valley as a function of k_{FE} whereby the other model parameters were taken along the valley indicated by the black line. The red line was placed at $\chi^2 + \delta\chi^2$, where $\delta\chi^2$ represents the uncertainty in χ^2 as determined by the root-mean square deviation between the linear fit of the experimental data (see Figure 1, black dots) and the actual data.

magnetic dipolar $^{15}N-^{1}H$ and $^{13}C-^{1}H$ vs ^{2}H nuclear quadrupolar interactions). However, this does not preclude that the minimization can get stuck in a local minimum belonging to the wrong regime. To address this potential issue, we also performed a minimization with initial values in the fast regime using both the two-state and three-state model. As expected, the optimization yielded a different local minimum, but with a substantially worse fit, as the χ^2 scoring parameter increases by 5.5-fold for the two-state model and by 390-fold for the three-state model. The principle cause of this increased χ^2 scoring parameter is the inadequate ratio between $\Delta R_+(^2H)$, $\Delta\Gamma(^{13}C)$, and $\Delta R_2(^{15}N)$ at $S^2 = 1$, thereby ruling out the fast regime for ubiquitin.

The complexity and CPU time-intensive nature of the SLE method preclude standard forms of error analysis, such as error propagation or Monte Carlo simulations. However, more detailed analysis of the fitting trajectory, seen in Figure 3, reveals a high degree of correlation among pairs fitting parameters in the low scoring χ^2-parameter space. This is indicative of a valley-shaped region of highly degenerate χ^2 scores, where a change in one fitting parameter will affect others with minimal effect on χ^2. This property is visualized by black lines in Figure 3. It suggests that any error in the initial fitting will cause a perturbation along this valley, and thus, the error in fitting can be extrapolated from the error in scoring parameter χ^2, which is plotted along the valley floor in the insert of Figure 3 (Panel A). Because the experimental NASR values deviate from a best-fit line by an amount significantly larger than their experimental error, we define the uncertainty in χ^2 based on the RMSD between the experimental NASR values and the best linear fit. This results in an uncertainty in the final score of $\delta\chi^2 = 0.005$, indicated by a horizontal red line in Figure 3A, which translates to an uncertainty in the free-to-encounter exchange rate $k_{ex,FE}$ of 660 s^{-1}. This can be translated to uncertainties of the other model parameters listed in Table 1.

In addition to obtaining a more detailed and more quantitative understanding of nanoparticle−protein interactions, the unified interpretation of NASR data for different relaxation processes provides a better understanding of the sensitivity of NASR to the time scales of internal protein dynamics. For this purpose, in Figure 4, dependence of the ratio $\rho = \Delta R(S^2 = 0.5)/\Delta R(S^2 = 1.0)$ is monitored as a function of the internal correlation time for the three-state binding model with the best-fit model parameters of Table 1. It shows that NASR of ubiquitin reflects time scales of internal motions over the range from 1 ps to 1 μs whereby the presence of the three-state exchange with the exchange parameters found for ubiquitin causes the extracted S^2(NASR) after global scaling to overestimate the true S^2 by about 30% $[\Delta\Gamma(^{13}C)]$, 32% $[\Delta R_2(^{15}N)]$, and 36% $[\Delta R_+(^{2}H)]$. These results corroborate and quantify the utility of NASR to access nanosecond to sub-microsecond internal motion time scales not accessible by standard NMR relaxation methods. At the same time, the precise exchange rate(s) of the protein to and from the nanoparticles can cause a reduction of the dynamic range of S^2, an effect that is most pronounced for methyl-side chain dynamics using ^{2}H relaxation as observed previously.[32] Fortunately, even for proteins for which a large set of complementarity NASR data are not available, and hence the

https://doi.org/10.1021/acs.jpcb.2c05967
J. Phys. Chem. B 2022, 126, 9089−9094

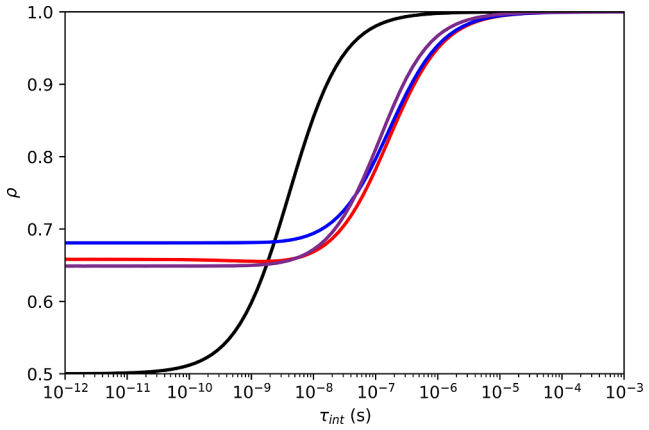

Figure 4. Ratio $\rho = \Delta R(S^2 = 0.5)/\Delta R(S^2 = 1.0)$ plotted as a function of internal correlation time τ_{int} for $\Delta R_+(^2H)$ (blue), $\Delta\Gamma(^{13}C)$ (purple), and $\Delta R_2(^{15}N)$ (red) for the best fit three-state model parameters in Table 1. The normalized spectral density function $J(0)$ is plotted in black, highlighting the different time-scale dependencies of classical spin relaxation (black) and NASR (colored).

quantitative parametrization of a multistate binding model is not feasible, useful information about internal dynamics can be extracted without SLE by establishing the relationship ΔR versus S^2 for residues belonging to well-defined secondary structures undergoing fast sub-nanosecond dynamics, allowing the straightforward identification of protein parts that undergo slower time scale motions. The exchange parameters determined here between ubiquitin and the anionic silica nanoparticles are likely to depend both on the specific properties of ubiquitin and the nanoparticles used. Systematic variation of the experimental conditions, such as buffer, pH, and temperature, should allow modification and further optimization of the internal protein dynamics observation window on the nano- to microsecond time scale by NASR.

This work is not intended to be an exhaustive exploration of protein−nanoparticle binding models to explain NASR data along with their limitations. Rather, we demonstrate that a simple two-state free-bound model is insufficient and that a physically intuitive sequential model with a third, intermediate state is able to describe the extensive body of experimental data accurately. Alternative, more sophisticated models may exist that are also able to adequately explain the NASR data. For example, it is quite possible that there exists a gradual (continuous) slowdown in the rotational rate of the protein as it approaches the nanoparticle. Alternatively, dynamic light scattering and TEM have indicated that the nanoparticles used have a size distribution with a finite width, and this dispersal in size of the bound state may partially contribute to the discrepancy between theoretical and experimental NASR results.[10,11]

Finally, a brief discussion of this work in the context of other recent nanoparticle−ligand interaction studies is in order. The finite offset in ΔR described above for ubiquitin has also been observed in a methyl-NASR study of colicin immunity protein Im7 interacting with silica nanoparticles.[32] The three-state binding pathway has been observed previously in DEST experiments on huntingtin peptides and TiO_2 nanoparticles[36] and on cholic acid and ceria nanoparticles.[35] This suggests transferability of the three-state behavior to potentially many other nanoparticle−ligand systems. Additionally, the principal strength of NASR lies in the observation of residue-specific dynamics on the nanosecond to microsecond time scale. These effects are identified through lower ΔR values than would be predicted by their traditional S^2 values. As the effects discussed in this paper are global while conserving the continuous, curved relationship between S^2 and ΔR, the identification of residues undergoing dynamics on such time scales is not impacted. Still, the increased complexity of the relationship between S^2 and ΔR reported here suggests that a fully quantitative analysis of nanosecond to microsecond time scale effects may require a nanoparticle−protein-specific SLE-based model to obtain the best quantitative interpretation of these residue-specific dynamic effects.

CONCLUSIONS

In this work, we developed and discussed two dynamic nanoparticle binding models for the quantitative interpretation of an extensive set of NASR data based on a SLE. We demonstrated that a two-state model representing solely the free and bound states is unable to simultaneously explain all our NASR data in a quantitative manner. However, the introduction of a third (encounter) state is sufficient to describe our data with good accuracy. We also reported a method to estimate the uncertainties of the three-state model parameters in spite of the complex nature of the underlying SLE.

AUTHOR INFORMATION

Corresponding Author

Rafael Brüschweiler − *Department of Chemistry and Biochemistry, The Ohio State University, Columbus, Ohio 43210, United States; Department of Biological Chemistry and Pharmacology, The Ohio State University, Columbus, Ohio 43210, United States;* orcid.org/0000-0003-3649-4543; Email: bruschweiler.1@osu.edu

Authors

Gregory Jameson − *Department of Chemistry and Biochemistry, The Ohio State University, Columbus, Ohio 43210, United States*

Xinyao Xiang − *Department of Chemistry and Biochemistry, The Ohio State University, Columbus, Ohio 43210, United States;* orcid.org/0000-0002-8584-3642

Complete contact information is available at: https://pubs.acs.org/10.1021/acs.jpcb.2c05967

Notes

The authors declare no competing financial interest.

ACKNOWLEDGMENTS

We thank Drs. Alexandar L. Hansen, Bruschweiler-Li, and Chunhua Yuan for helpful discussions and comments on the manuscript. This work was supported by the U.S. National Science Foundation (grant MCB-2103637).

REFERENCES

(1) Li, Z.; Barnes, J. C.; Bosoy, A.; Stoddart, J. F.; Zink, J. I. Mesoporous silica nanoparticles in biomedical applications. *Chem. Soc. Rev.* **2012**, *41*, 2590−2605.

(2) Mitragotri, S.; Anderson, D. G.; Chen, X.; Chow, E. K.; Ho, D.; Kabanov, A. V.; Karp, J. M.; Kataoka, K.; Mirkin, C. A.; Petrosko, S. H.; et al. Accelerating the translation of nanomaterials in biomedicine. *ACS Nano* **2015**, *9*, 6644−6654.

(3) Nel, A. E.; Mädler, L.; Velegol, D.; Xia, T.; Hoek, E. M.; Somasundaran, P.; Klaessig, F.; Castranova, V.; Thompson, M. Understanding biophysicochemical interactions at the nano-bio interface. *Nat. Mater.* **2009**, *8*, 543−557.
(4) Kim, S. T.; Saha, K.; Kim, C.; Rotello, V. M. The role of surface functionality in determining nanoparticle cytotoxicity. *Acc. Chem. Res.* **2013**, *46*, 681−691.
(5) Kelly, P. M.; Åberg, C.; Polo, E.; O'Connell, A.; Cookman, J.; Fallon, J.; Krpetić, Ž.; Dawson, K. A. Mapping protein binding sites on the biomolecular corona of nanoparticles. *Nat. Nanotechnol.* **2015**, *10*, 472−479.
(6) Monopoli, M. P.; Åberg, C.; Salvati, A.; Dawson, K. A. Biomolecular coronas provide the biological identity of nanosized materials. *Nat. Nanotechnol.* **2012**, *7*, 779−786.
(7) Docter, D.; Westmeier, D.; Markiewicz, M.; Stolte, S.; Knauer, S. K.; Stauber, R. H. The nanoparticle biomolecule corona: lessons learned − challenge accepted? *Chem. Soc. Rev.* **2015**, *44*, 6094−6121.
(8) Ceccon, A.; Tugarinov, V.; Bax, A.; Clore, G. M. Global dynamics and exchange kinetics of a protein on the surface of nanoparticles Revealed by Relaxation-Based Solution NMR Spectroscopy. *J. Am. Chem. Soc.* **2016**, *138*, 5789−5792.
(9) Xie, M.; Yu, L.; Bruschweiler-Li, L.; Xiang, X.; Hansen, A. L.; Brüschweiler, R. Functional protein dynamics on uncharted time scales detected by nanoparticle-assisted NMR spin relaxation. *Sci. Adv.* **2019**, *5*, No. eaax5560.
(10) Wardenfelt, S.; Xiang, X.; Xie, M.; Yu, L.; Bruschweiler-Li, L.; Brüschweiler, R. Broadband dynamics of ubiquitin by anionic and cationic nanoparticle assisted NMR spin relaxation. *Angew. Chem., Int. Ed.* **2021**, *60*, 148−152.
(11) Xie, M.; Hansen, A. L.; Yuan, J.; Brüschweiler, R. Residue-specific interactions of an intrinsically disordered protein with silica nanoparticles and their quantitative prediction. *J. Phys. Chem. C* **2016**, *120*, 24463−24468.
(12) Zanzoni, S.; Pedroni, M.; D'Onofrio, M.; Speghini, A.; Assfalg, M. Paramagnetic nanoparticles leave their mark on nuclear spins of transiently adsorbed proteins. *J. Am. Chem. Soc.* **2016**, *138*, 72−75.
(13) Calvaresi, M.; Arnesano, F.; Bonacchi, S.; Bottoni, A.; Calò, V.; Conte, S.; Falini, G.; Fermani, S.; Losacco, M.; Montalti, M.; et al. C_{60}@Lysozyme: direct observation by nuclear magnetic resonance of a 1:1 fullerene protein adduct. *ACS Nano* **2014**, *8*, 1871−1877.
(14) Shrivastava, S.; McCallum, S. A.; Nuffer, J. H.; Qian, X.; Siegel, R. W.; Dordick, J. S. Identifying specific protein residues that guide surface interactions and orientation on silica nanoparticles. *Langmuir* **2013**, *29*, 10841−10849.
(15) Xie, M.; Li, D.-W.; Yuan, J.; Hansen, A. L.; Brüschweiler, R. Quantitative binding behavior of intrinsically disordered proteins to nanoparticle surfaces at individual residue level. *Chem.—Eur. J.* **2018**, *24*, 16997−17001.
(16) Li, D.-W.; Xie, M.; Brüschweiler, R. Quantitative cooperative binding model for intrinsically disordered proteins interacting with nanomaterials. *J. Am. Chem. Soc.* **2020**, *142*, 10730−10738.
(17) Tira, R.; De Cecco, E.; Rigamonti, V.; Santambrogio, C.; Barracchia, C. G.; Munari, F.; Romeo, A.; Legname, G.; Prosperi, D.; Grandori, R.; et al. Dynamic molecular exchange and conformational transitions of alpha-synuclein at the nano-bio interface. *Int. J. Biol. Macromol.* **2020**, *154*, 206−216.
(18) Randika Perera, Y.; Hill, R. A.; Fitzkee, N. C. Protein interactions with nanoparticle surfaces: highlighting solution NMR techniques. *Isr. J. Chem.* **2019**, *59*, 962−979.
(19) Ceccon, A.; Tugarinov, V.; Boughton, A. J.; Fushman, D.; Clore, G. M. Probing the binding modes of a multidomain protein to lipid-based nanoparticles by relaxation-based NMR. *J. Phys. Chem. Lett.* **2017**, *8*, 2535−2540.
(20) Favro, L. D. Theory of the rotational brownian motion of a free rigid body. *Phys. Rev.* **1960**, *119*, 53−62.
(21) Ni, F. Recent developments in transferred NOE methods. *Prog. Nucl. Magn. Reson. Spectrosc.* **1994**, *26*, 517−606.
(22) Post, C. B. Exchange-transferred NOE spectroscopy and bound ligand structure determination. *Curr. Opin. Struct. Biol.* **2003**, *13*, 581−588.
(23) Halle, B.; Denisov, V. P.Magnetic relaxation dispersion studies of biomolecular solutions. In *Methods in Enzymology*; James, T. L., Dötsch, V., Schmitz, U., Eds.; Academic Press, 2002; Vol. *338*, pp 178−201.
(24) Bertini, I.; Fragai, M.; Luchinat, C.; Talluri, E. Water-based ligand screening for paramagnetic metalloproteins. *Angew. Chem., Int. Ed.* **2008**, *47*, 4533−4537.
(25) Mayer, M.; Meyer, B. Characterization of ligand binding by saturation transfer difference NMR spectroscopy. *Angew. Chem., Int. Ed.* **1999**, *38*, 1784−1788.
(26) Angulo, J.; Nieto, P. M. STD-NMR: application to transient interactions between biomolecules—a quantitative approach. *Eur. Biophys. J.* **2011**, *40*, 1357−1369.
(27) Clore, G. M.; Iwahara, J. Theory, practice, and applications of paramagnetic relaxation enhancement for the characterization of transient low-population states of biological macromolecules and their complexes. *Chem. Rev.* **2009**, *109*, 4108−4139.
(28) Clore, G. M.; Tang, C.; Iwahara, J. Elucidating transient macromolecular interactions using paramagnetic relaxation enhancement. *Curr. Opin. Struct. Biol.* **2007**, *17*, 603−616.
(29) Fawzi, N. L.; Ying, J.; Ghirlando, R.; Torchia, D. A.; Clore, G. M. Atomic-resolution dynamics on the surface of amyloid-β protofibrils probed by solution NMR. *Nature* **2011**, *480*, 268−272.
(30) Anthis, N. J.; Clore, G. M. Visualizing transient dark states by NMR spectroscopy. *Q. Rev. Biophys.* **2015**, *48*, 35−116.
(31) Jameson, G.; Brüschweiler, R. NMR spin relaxation theory of biomolecules undergoing highly asymmetric exchange with large interaction partners. *J. Chem. Theory Comput.* **2021**, *17*, 2374−2382.
(32) Xiang, X.; Hansen, A. L.; Yu, L.; Jameson, G.; Bruschweiler-Li, L.; Yuan, C.; Brüschweiler, R. Observation of sub-microsecond protein methyl-side chain dynamics by nanoparticle-assisted NMR spin relaxation. *J. Am. Chem. Soc.* **2021**, *143*, 13593−13604.
(33) Abragam, A.*The Principles of Nuclear Magnetism*; Clarendon Press, 1961.
(34) Gao, F.; Han, L. Implementing the Nelder-Mead simplex algorithm with adaptive parameters. *Comput. Optim. Appl.* **2012**, *51*, 259−277.
(35) Egner, T. K.; Naik, P.; Nelson, N. C.; Slowing, I. I.; Venditti, V. Mechanistic insight into nanoparticle surface adsorption by solution NMR spectroscopy in an aqueous gel. *Angew. Chem., Int. Ed.* **2017**, *56*, 9802−9806.
(36) Ceccon, A.; Tugarinov, V.; Clore, G. M. TiO_2 nanoparticles catalyze oxidation of huntingtin exon 1-derived peptides impeding aggregation: a quantitative NMR study of binding and kinetics. *J. Am. Chem. Soc.* **2019**, *141*, 94−97.
(37) Rabani, R.; Saidi, M. H.; Joly, L.; Merabia, S.; Rajabpour, A. Enhanced local viscosity around colloidal nanoparticles probed by equilibrium molecular dynamics simulations. *J. Chem. Phys.* **2021**, *155*, 174701.
(38) Alberty, R. A.; Hammes, G. G. Application of the Theory of Diffusion-controlled Reactions to Enzyme Kinetics. *J. Phys. Chem.* **1958**, *62*, 154−159.

https://doi.org/10.1021/acs.jpcb.2c05967
J. Phys. Chem. B 2022, 126, 9089−9094